

PART IV: HYDRODYNAMICS ASPECTS OF THE ELECTROKINETIC REMEDIATION PROCESS IN THE NEAR THE ELECTRODES ZONE: BOUNDARY LAYER APPROACH TO ELECTRO-MECHANISMS AND JOULE HEATING

Chapter IX. Electrodes of Rectangular Geometry

9.1 Introduction and Motivation

Electrokinetic applications of soil remediation are a promising technology that needs more understanding of the different phenomena occurring during operation. Different arrangements of the same technology tend to favor different and specific mechanisms that usually drive the mass transfer and/or the hydrodynamics of the system. The intrinsic complexity of electrokinetic remediation inhibits the scaling of conceptual designs to field applications. This is aggravated by the fact that there seems to be a science gap between field applications and the set of supporting fundamental equations, valid sources of design and process optimization. Therefore, the authors have undertaken a line of research where modeling can be a useful tool to unveil important practical questions. Furthermore, the strategy used is to isolate important components of the electrokinetic system and develop a pertinent analysis and study.

An electrokinetic cell can be divided in two main zones of interest; this is the treatment zone and the electrodes zone. In particular, this last mentioned region becomes the focus of attention in processes where the location of the ultimate chemical reaction and the point of fluid extraction are near the electrodes. Electrokinetic remediation methodologies, in

which this particular zone is a key for technology success, are for example Cation Selective Membrane, Ceramic Casting, Electrochemical ion exchange and specific cases of Lasagna process. As a consequence, knowing the hydrodynamics of the system, for example, in such an important region is highly desired. Furthermore, it is of great interest to know the effect of other mechanisms that come into play when greater differential potentials are applied. Among these mechanisms are the convective and buoyancy forces not yet considered and reported in the literature.

The lack of fundamental information on the engineering science part of electrokinetic systems has caused misconceptions about the ability of an electrical field to produce good results under particular soil conditions. Several variables are reported as controlling removal. In some instances, water content as well as pH is believed to be responsible for removal efficiency. Precisely, this is the case of Ceramic Casting where in a controlled volume of contaminated soil, a buffered solution is added to ensure a constant value of water content and pH. This particular case involves mass transfer and is the subject matter of a future investigation. However, there is another important controlling variable; this is the Joule heating effect which is equally responsible for removal efficiency, although not necessarily well understood.

Several authors have reported temperature developments on electrokinetic processes of soil remediation during operation. One of them, for example, reports that the electroosmotic mechanism seems to be affected when temperature rises and as a result low process efficiency is obtained (Yeung et al., 1997). Conversely, increase of temperature is reported beneficial to the fluid dynamic of hydrocarbon-containing fluids in that their viscosity is reduced (Chilingar et al., 1997). To introduce more conflicting ideas, overheating is recognized as an operational phenomenon that has to be avoided (Lageman, 1993; Ho et al., 1997). And finally, it has been concluded that one of the disadvantages of electrokinetic remediation is that an increment of temperature produces a decrement of process efficiency (Virkutyle et al., 2002). Perhaps, as a working hypothesis, all these researchers are facing identical phenomena but not necessarily taking the best advantage of them. Therefore it is urgent to explain the proposed phenomenon through basic engineering science; in particular,

the role of temperature during the electrokinetic remediation. This would allow researchers and practitioners to better understand the process, new technology approaches can be implemented, optimal operation parameters can be obtained, and alternative and cost efficient process can be applied.

The focus of this chapter is the role of the Joule heating effect in the near electrodes zone. In other words, this chapter promotes basic understanding of the effects of heat generation on removal efficiency of electrokinetic remediation applications. The investigation focuses on specialized cases of boundary layer flows, with low Reynolds number, in vertical electrodes of rectangular geometry. Also, one of the purposes of this chapter is to promote understanding of the behavior of the velocity field near the electrode in electro-remediation. The study uses several assumptions to achieve the goals; however, it is believed that key aspects of the heat generation in the electrokinetic remediation processes are captured.

9.2 Modeling Approach

The characteristics of the problem described above suggest that the best modeling approach is a boundary layer analysis. This methodology was applied in a similar study conducted by Turnbull (1969) who discusses the effects of an electric field across the flow of a fluid but neglecting any form of heat generation (source term). Furthermore, Turnbull (1969) included electric fields in the Navier-Stokes equations, energy equation, and mass transfer equations. This author used the Von Karman boundary layer approximation to obtain his final solution. The Von Karman's method has been very well documented and particularly applied in heat transfer processes (Whitaker, 1983). The approach utilized by Turnbull, to solve the system, is of particular interest to investigate the electrokinetic problem. In fact, this approach can be adapted to investigate the heat generation problem, previously mentioned, characteristic of electroremediation. In this case, the most important difference with Turnbull's approach is that the source term due to Joule heating is included and its role on the hydrodynamic field is systematically investigated. Also, the boundary conditions have been modified to fit the specificities normally given in an electroremediation electrode system.

9.3 System Description

The system been analyzed corresponding to a vertical electrode of rectangular geometrical aspect. This vertical plate, electrode, presents a 3D characteristic that has been simplified to a 2D system since the depth presents no variation. In other words, the most important coordinates of the system are the axial, x-direction, and the transversal, y-direction. The electrode surface in contact with the fluid presents a constant temperature T_0 while the fluid outside the boundary layer region has uniform temperature T_∞ . The temperature difference between the wall surface of the electrode and the fluid causes buoyancy driven flows to take place as a thin boundary layer moving tangential to the vertical plate. In particular, the buoyancy phenomenon, also known as free convection, is promoted by density variations proportional to the aforementioned temperature difference.

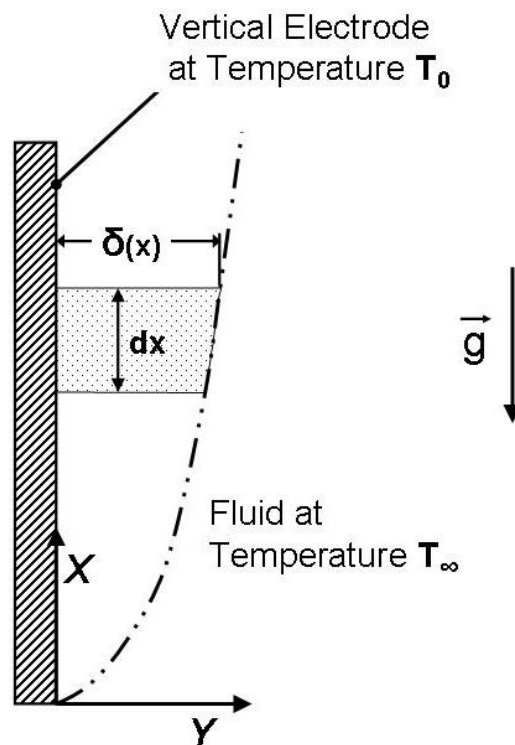


Figure 9.1 Control volume and main variables associated with the boundary layer flow in a flat electrode geometry.

In addition, an applied electrical field, E , in the transversal direction (i.e., the y -axis) of the vertical electrode is present. As the fluid inside the boundary layer presents a non-zero resistance to the electrical current, heat generation takes place due to the Joule heating effect. For this study, the generated heat of magnitude Q is assumed constant with time and uniform across the layer. This additional thermal stress could modify further more the hydrodynamic inside the boundary layer of fluid near the vertical wall. In physicochemical terms, the fluid, as described above, is assumed Newtonian, incompressible for the mass conservation aspects and under steady state conditions. Furthermore, the Boussinesq (Gebhart et al., 1988) assumption is considered valid in the analysis; this is the fluid has constant properties everywhere except for the density in the buoyancy force term.

9.4 Model Formulation

The preceding description of the system being studied calls for the analysis of temperature and velocity profiles inside the boundary layer. The fundamental expressions that model the system as presented are the energy and motion equations. In the present section, these two equations are developed as the heat transfer and hydrodynamic models. However, the use of the continuity equation is crucial to construct the differential mathematical models herein intended.

9.4.1 Heat Transfer Model

The transfer problem for the system under study invokes the energy conservation equation (Bird et al., 1960). A similar approach, undertaken by Squire (1938) and Turnbull (1969), was developed for the case of fluid with low electric resistance. Taking this approach as a basis and including the heat generation term in the conservation of energy equation, the following equation is obtained:

$$\rho \cdot C_p \frac{DT}{Dt} = \nabla \cdot (k \cdot \nabla T) + Q \quad (9.1)$$

where D is used to indicate the convective derivative, Q is the heat generation due to the Joule heating effect, ρ the fluid density, C_p the specific heat, and k the thermal conductivity of the fluid.

Using dimensionless variables, i.e., transforming from X, Y coordinate system to a non-dimensional ξ, η system, the following single parameter expressions are introduced:

Characteristic Length

$$L = \left[\frac{\mu^2}{\rho_0^2 \cdot g \cdot \beta \cdot (T_0 - T_\infty)} \right]^{1/3} \quad (9.2)$$

Thermal Velocity

$$v_T = \frac{k}{\rho \cdot C_p} \frac{1}{L} ; \quad v_T = \alpha_D \frac{1}{L} \quad (9.3)$$

where μ is the fluid viscosity, β the compressibility coefficient and α_D the thermal diffusivity.

The following additional definitions of dimensionless variables are also necessary to fully convert the energy equation to dimensionless variables.

$$v_x^+ = \frac{v_x}{v_T} \quad (9.4a)$$

$$v_y^+ = \frac{v_y}{v_T} \quad (9.4b)$$

$$\theta = \frac{T - T_\infty}{T_0 - T_\infty} \quad (9.4c)$$

$$\phi^2 \equiv \frac{Q \cdot L^2}{k \cdot (T_0 - T_\infty)} \quad (9.4d)$$

$$\xi = \frac{x}{L} \quad (9.4e)$$

$$\eta = \frac{y}{L} \quad (9.4f)$$

By substituting the parameters and variables previously identified in equation 9.1, the following non-dimensional differential equation is obtained for the energy balance.

$$v_x^+ \cdot \frac{\partial \theta}{\partial \xi} + v_y^+ \cdot \frac{\partial \theta}{\partial \eta} = \frac{\partial^2 \theta}{\partial \eta^2} + \phi^2 \quad (9.5)$$

This form of the energy equation is obtained under the steady state conditions, boundary layer approximation and the fact that conduction is assumed important only in the transversal direction for the system shown in Figure 9.1.

9.4.2 The Continuity Equation

Another fundamental principle that must be considered in the system is the irreversible conversion of thermal energy in momentum. In fact, the 2D geometry of the system obligates this inclusion. This principle comes in the form of the continuity equation for incompressible flow situations; this is $\nabla \cdot \mathbf{v} = 0$ (Bird et al., 1960, Whitaker, 1983). Therefore, for the case of incompressible flow, under the Boussinesq assumption, the following is the expression in rectangular coordinates.

$$\frac{\partial V_x}{\partial x} + \frac{\partial V_y}{\partial y} = 0 \quad (9.6a)$$

or in the dimensionless terms,

$$\frac{\partial V_x^+}{\partial \xi} + \frac{\partial V_y^+}{\partial \eta} = 0 \quad (9.6b)$$

9.4.3 Hydrodynamic Model

The hydrodynamic part of the system, as described in section 9.3, could be perfectly modeled by the Navier-Stokes equation (Whitaker, 1983). This is a direct consequence of having assumed that the fluid has a Newtonian behavior. However, to simplify the analysis in this first effort, none of the electro-mechanisms that normally affect the hydrodynamic field are considered. The invoked theoretical expression is given by

$$\rho \frac{D\mathbf{v}}{Dt} = -\nabla p + \mu \cdot \nabla^2 \mathbf{v} + \rho \cdot \mathbf{g} \quad (9.7)$$

where \mathbf{g} is the gravitational constant, p is the pressure, and μ is the fluid viscosity. The density ρ , as described in previous chapters, is a function of temperature. To compute the density term, a first order Taylor approximation around a reference temperature T_∞ of the system is applied (Bird et al., 1960, Turnbull, 1969), given by:

$$\rho(T) = \rho(T_\infty) [1 - \beta_\infty \cdot (T - T_\infty)] \quad (9.8)$$

and where β_∞ is the volumetric compressibility of the fluid at a reference temperature T_∞ , in this case the fluid temperature away for the surface of the electrode.

The Navier-Stokes equation (Bird et al, 1960), equation 9.7, can be written in the respective Cartesian components in x (ξ) and y (η) directions of the system.

Coordinate x :

$$\rho_\infty \cdot \left(v_x \cdot \frac{\partial v_x}{\partial \xi} + v_y \cdot \frac{\partial v_x}{\partial \eta} \right) = -\frac{\partial p}{\partial x} - \mathbf{g} \cdot \rho_\infty \cdot [1 - \beta_\infty \cdot (T - T_\infty)] + \mu \cdot \left(\frac{\partial^2 v_x}{\partial \xi^2} + \frac{\partial^2 v_x}{\partial \eta^2} \right) \quad (9.9a)$$

$$v_x^+ \cdot \frac{\partial v_x^+}{\partial \xi} + v_y \cdot \frac{\partial v_x^+}{\partial \eta} = \frac{1}{\text{Re}} \left(\frac{\partial^2 v_x^+}{\partial \xi^2} + \frac{\partial^2 v_x^+}{\partial \eta^2} \right) + \frac{\text{Gr}}{\text{Re}^2} \theta \quad (9.9b)$$

Coordinate y:

$$\rho_{\infty} \cdot \left(v_x \cdot \frac{\partial v_y}{\partial \xi} + v_y \cdot \frac{\partial v_x}{\partial \eta} \right) = +\mu \cdot \left(\frac{\partial^2 v_y}{\partial \xi^2} + \frac{\partial^2 v_x}{\partial \eta^2} \right) \quad (9.10a)$$

$$v_x^+ \cdot \frac{\partial v_y^+}{\partial \xi} + v_y^+ \cdot \frac{\partial v_x^+}{\partial \eta} = \frac{1}{\text{Re}} \left(\frac{\partial^2 v_y^+}{\partial \xi^2} + \frac{\partial^2 v_x^+}{\partial \eta^2} \right) \quad (9.10b)$$

where the following definition of dimensionless numbers applies

$$\text{Gr} = \frac{\rho_{\infty}^2 \cdot g \cdot \beta_{\infty} \cdot (T_0 - T_{\infty}) \cdot L^3}{\mu^2} \quad (9.11a)$$

$$\text{Re} = \frac{\rho_{\infty} \cdot v_T \cdot L}{\mu} \quad (9.11b)$$

The Grashoff number, Gr, represents the buoyancy to viscous forces due to changes in temperature and density respectively. This free convective phenomenon is shown in equation 9.9 a&b. On the other hand, the Reynolds number, Re, represents the inertia to viscous forces. The Reynolds effect can be observed in both coordinate components, equation 9.9 (a&b) and 9.10 (a&b).

Following closely the methodology applied by Turnbull (1969) over equations 9.9b and 9.10b, with the modifications herein proposed, is that the usual boundary layer approximations will be made to construct differential mathematical models. In particular, the partial derivative of equations 9.9b and 9.10b with respect to orthogonal coordinates can be combined and reduced using the continuity equation 9.6b to yield the following differential expression:

$$v_x^+ \cdot \left(\frac{\partial^2 v_y^+}{\partial \xi^2} + \frac{\partial^2 v_x^+}{\partial \eta^2} \right) - v_y^+ \cdot \left(\frac{\partial^2 v_x^+}{\partial \xi^2} + \frac{\partial^2 v_y^+}{\partial \eta^2} \right) = \frac{1}{\text{Re}} \left(\frac{\partial^3 v_y^+}{\partial \xi^3} + \frac{\partial^3 v_y^+}{\partial \xi \partial \eta^2} - \frac{\partial^3 v_x^+}{\partial \xi^2 \partial \eta} - \frac{\partial^3 v_x^+}{\partial \eta^3} \right) - \frac{\text{Gr}}{\text{Re}^2} \theta \quad (9.12)$$

Equation 9.12 can be further simplified if the order of magnitude of the derivative with respect to transversal coordinate is assumed to be much larger than the one of the derivatives with respect to axial (Whitaker, 1983); this is

$$\frac{\partial(\bullet)}{\partial\eta} \gg \frac{\partial(\bullet)}{\partial\xi} \quad (9.13)$$

This assumption is justified since the width of the boundary layer, δ , is much smaller than any characteristic dimension in the x-direction. In addition, the magnitude of the velocity component, V_x , is considered to be much larger than the one of the other velocity component, V_y .

After applying the simplification suggested by equation 9.13 on equation 9.12 the following expression can be obtained:

$$v_x^+ \cdot \frac{\partial^2 v_y^+}{\partial\eta^2} - v_y^+ \cdot \frac{\partial^2 v_x^+}{\partial\eta^2} = -\frac{1}{\text{Re}} \frac{\partial^3 v_x^+}{\partial\eta^3} - \frac{\text{Gr}}{\text{Re}^2} \theta \quad (9.14)$$

Equation 9.14 can be integrated with respect to the transversal coordinate, using equation 9.6b in the procedure. The following expression is derived this calculus operation has been performed:

$$v_x^+ \cdot \frac{\partial v_x^+}{\partial\xi} + v_y^+ \cdot \frac{\partial v_x^+}{\partial\eta} = \frac{1}{\text{Re}} \frac{\partial^2 v_x^+}{\partial\eta^2} + \frac{\text{Gr}}{\text{Re}^2} \theta - \chi \quad (9.15)$$

where χ is an integration constant. To compute χ , Turnbull (1969) utilized as the boundary condition the bulk fluid of the system. This condition has been changed in this thesis and therefore the surface wall region of the electrode must be considered. In this domain the magnitude of the velocity profile is zero and the temperature of the fluid is uniform and given by T_0 . Therefore, after evaluating the equation 9.15 in the suggested boundary condition, χ is obtained.

$$\chi = \frac{\text{Gr}}{\text{Re}^2} \quad (9.16)$$

In equation 9.16, χ shows no dependence of the axial coordinate, but with buoyancy through the Grashoff number. A simple substitution of the χ expression on equation 9.15 yields the final differential expression for the velocity field, the hydrodynamic model:

$$v_x^+ \cdot \frac{\partial v_x^+}{\partial \xi} + v_y \cdot \frac{\partial v_x^+}{\partial \eta} = \frac{1}{\text{Re}} \frac{\partial^2 v_x^+}{\partial \eta^2} + \frac{\text{Gr}}{\text{Re}^2} (\theta - 1) \quad (9.17)$$

where all the terms have been previously identified.

9.5 Derivation of Von Karman Integral Approximation

At their current stage, equations 9.5 and 9.17, the heat transfer and hydrodynamic models respectively, have no trivial mathematical or numerical solution. In addition, boundary conditions need to be defined. To overcome these limitations, the Von Karman integral approximation will be applied in the analysis of the boundary layer. The application of the Von Karman method on equations 9.5 and 9.17 inverts the partial differential equation system, first, to an integro-differential model and then into a two-equation ordinary differential model (Whitaker, 1981). This task is accomplished below.

Equations 9.5 and 9.17 need to be integrated over the transversal variable (y or η , see Figure 9.1) from the electrode wall surface (i.e., $y = 0$, or $\eta=0$) to the edge of the boundary layer, (i.e., $y=\delta$, or $\eta= \delta^+$). The conditions for the velocity and temperature fields involved in these integrals are

$$V_x^+ = V_y^+ = 0 \quad @ \quad \eta = 0, \delta^+ \quad (9.18a)$$

$$\theta = 1 \quad @ \quad \eta = 0 \quad (9.18b)$$

$$\theta = 0 \quad @ \quad \eta = \delta^+ \quad (9.18c)$$

In the suggested mathematical operation, it must be considered that ϕ^2 is constant in the transversal direction, across the boundary layer thickness. As a result, the following integro-differential equations are derived

$$\frac{\partial}{\partial \xi} \int_0^{\delta^+} v_y^+ \cdot \theta \cdot \partial \eta = \int_0^{\delta^+} \frac{\partial^2 \theta}{\partial \eta^2} \cdot \partial \eta + \phi^2 \cdot \delta^+ \quad (9.19)$$

$$\frac{\partial}{\partial \xi} \int_0^{\delta^+} (v_y^+)^2 \cdot \partial \eta = \frac{1}{\text{Re}} \cdot \int_0^{\delta^+} \frac{\partial^2 v_x^+}{\partial \eta^2} \cdot \partial \eta + \frac{\text{Gr}}{\text{Re}^2} \cdot \int_0^{\delta^+} (\theta - 1) \cdot \partial \eta \quad (9.20)$$

which are the integral approximations for the energy and momentum equations with a uniform heat generation (due to the Joule effect) across the domain of the system.

The next step in the methodology requires approximate expressions for the velocity profile, V_x^+ , and for the temperature profile, θ , as functions of independent variables. In the analysis by Turnbull (1969), V_x^+ was obtained from a convective free-problem in the absence of an electric field. This approximation was initially proposed by Squire (1938) and it will be followed in this study. Therefore, the proposed dimensionless velocity profile is given by

$$V_x^+ = U^+ \cdot \frac{\eta}{\delta^+} \cdot \left(1 - \frac{\eta}{\delta^+}\right)^2 \quad (9.21)$$

where U^+ is the dimensionless velocity amplitude in the ξ -direction (x-direction) and δ^+ the dimensionless boundary layer thickness, both trivially obtained using the thermal velocity and characteristic length defined previously in section 9.4, above.

For temperature the following profile is used in this study to describe temperature variations in the boundary layer domain (Squire, 1938)

$$\theta = \left(1 - \frac{\eta}{\delta^+}\right)^2 \quad (9.22)$$

Continuing with Turnbull's approach, after a proper substitution of the proposed velocity and temperature profiles and integration are performed, the methodology yields the following two first-order differential equations:

$$\frac{\partial}{\partial \xi} \left(\frac{1}{30} \cdot U^+ \cdot \delta^+ \right) = \frac{2}{\delta^+} + \phi^2 \cdot \delta^+ \quad (9.23)$$

$$\frac{\partial}{\partial \xi} \left(\frac{1}{105} \cdot U^{+2} \cdot \delta^+ \right) = -\frac{2}{3} \cdot \frac{\text{Gr}}{\text{Re}^2} \cdot \delta^+ - \frac{1}{\text{Re}} \cdot \frac{U^+}{\delta^+} \quad (9.24)$$

These equations can be solved either numerically or analytically. The analytical solution has been developed somewhere else using as boundary condition the region of the bulk fluid of the system. The present thesis, however, concentrates on the numerical solution. Therefore, further algebraic development of equations 9.23 and 9.24 yields the following differential system and boundary conditions.

$$\frac{\partial U^+}{\partial \xi} = -\left(\frac{105}{\text{Re}} + 60\right) \left(\frac{1}{\delta^{+2}}\right) - 70 \cdot \frac{\text{Gr}}{\text{Re}^2} \left(\frac{1}{U^+}\right) + 30 \cdot \phi^2 \quad (9.25a)$$

$$\frac{\partial \delta^+}{\partial \xi} = \left(\frac{105}{\text{Re}} + 120\right) \left(\frac{1}{U^+ \cdot \delta^+}\right) + 70 \cdot \frac{\text{Gr}}{\text{Re}^2} \left(\frac{\delta^+}{U^{+2}}\right) - 60 \cdot \phi^2 \cdot \frac{\delta^+}{U^+} \quad (9.25b)$$

$$\delta^+ = 0 \quad @ \quad \xi = 0 \quad (9.25c)$$

$$U^+ = 0 \quad @ \quad \xi = 0 \quad (9.25d)$$

This model system, represented by equations 9.25 a-d, is trivially solved using conventional numerical methods. For simplicity reasons, the results reported in the next

section were obtained using Euler's method, sometimes called Heun's method (Kreyszing, 1999). The step size of iteration, required by the method, was kept small in order to avoid inaccuracy and imprecision problems.

9.6 Illustrative Results and Discussion

A set of figures describing different case scenarios are presented in this sub-section to facilitate the analysis of information. These figures are the result of applying and solving the differential expressions developed in the previous sub-section. The hydrodynamics taking place in the region near the electrode and the role of Joule heating is intended to be explained in this analysis. Therefore, plots for boundary layer thickness, temperature profiles, and for the components of the velocity field will be the focus of the discussion. To produce meaningful results for the system, a fluid of reference must be identified and, in this case, the physical properties of water have been chosen for such a purpose. This is necessary to calculate reasonable values of dimensionless numbers, Reynolds and Grashof, required by equations 25 a&b. In addition, these equations also require a value for the source generation term, ϕ^2 , for their solution. This particular requirement gives the opportunity to study the role of the heating effect being analyzed in this work. In consequence, a valid range of physical values must be defined. Positive values of ϕ^2 indicates heat generation, and therefore, the following range has been chosen

$$0 \leq \phi^2 \leq 5 \quad (9.26)$$

From the previous range and for analysis purposes, four ϕ^2 values have been selected as $\phi^2 = 0$, $\phi^2 = 1.5$, $\phi^2 = 3.0$, and $\phi^2 = 5.0$. The $\phi^2 = 0$ has been included as a reference value for the case of no Joule heating effect. On the other hand, the $\phi^2 = 5.0$ has been selected as a maximum considering that such a value produces an increase in the slope of the boundary layer near the origin of four times (300%) the values for the case of no Joule heating effect. The other two have been selected randomly. With the set of valid ϕ^2 illustration of

temperature profiles, boundary layer thickness, and velocity profiles have been made and they are presented next.

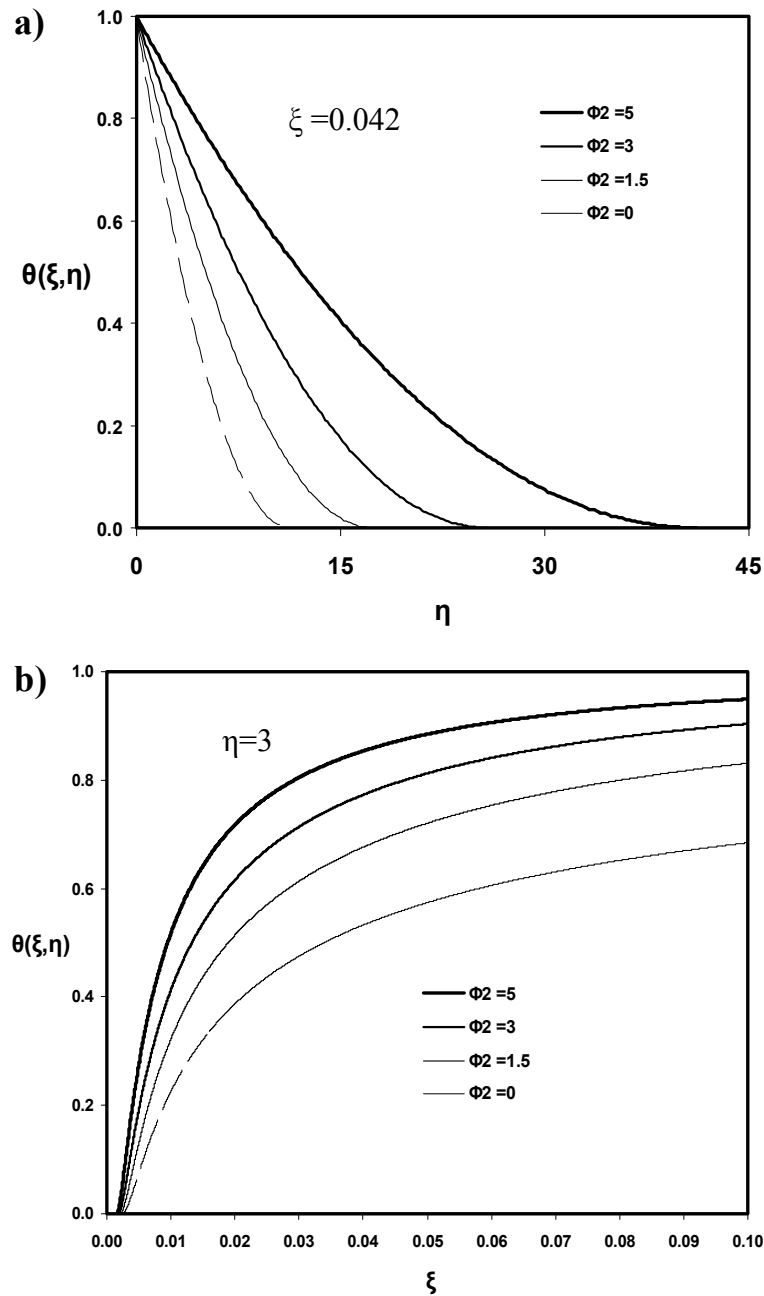


Figure 9.2 Dimensionless temperature profiles (inside the boundary layer) for various values of the heat generation source term. Case of $\xi=0.042$ for the η -direction (a) and case of $\eta = 3$ for the ξ -direction (b)

Figure 9.2 (a) shows parametric representation of the influence of Joule heating generation on temperature profiles inside the boundary layer domain. Furthermore, the figure shows that the range of acceptable ϕ^2 values produces a family of decay type curves. In particular, this figure illustrates temperature variation as a function of the transversal direction of the boundary layer (η) for a given value of axial direction, ($\xi=0.042$). For all given values of ϕ^2 the temperature at the surface of the electrode remain at the value of $\theta = 1$. Specifically, for a value of ϕ^2 equal to 5.0 the temperature has a variation between the values of $\theta = 1$, at the electrode surface, and a value of $\theta = 0$, i.e. fluid temperature, at $\eta=40$. A decrease in ϕ^2 values from 5.0 to 3 yields a reduction on the η value from 40 to 25 in order to reach the same fluid temperature. From a cross sectional analysis on $\eta=10$, the figure predicts that this 40% reduction in ϕ^2 value will cause a reduction of approximately 35% in temperature values. Further reduction in ϕ^2 values from 3.0 to 1.5 produces a decrease on the η value from 25 to 17 as to both obtain the fluid temperature. A similar trend as the one previously reported is observed on this 50% reduction in ϕ^2 that will cause a reduction of approximately 52% in temperature values. Therefore, the system temperature shows high sensitivity to the Joule heating effect.

Figure 9.2 (b) displays temperature variation along the axial coordinate ξ for a given position of η ($\eta=3$). A single identifiable trend along the axial coordinate, ξ , is clearly observed. For each value of ϕ^2 chosen within the defined domain, the temperature profiles describe an inverse exponential function of different amplitudes, respectively. The higher the value of ϕ^2 the wider is the amplitude of the curve. Additionally, near the electrode region ($\xi < 0.03$, approximately) steep variations in temperature values are developed in all cases to reach different plateau values beyond $\xi = 0.04$, approximately, with an incipient transition in between. This just described temperature behavior has been also identified in an analytical solution approach of this differential boundary layer model (see future work chapter). Nevertheless, the selection of a more stable boundary condition, as presented herein, yields results that more sharply define the reported trend observed in either the analytical and numerical solutions.

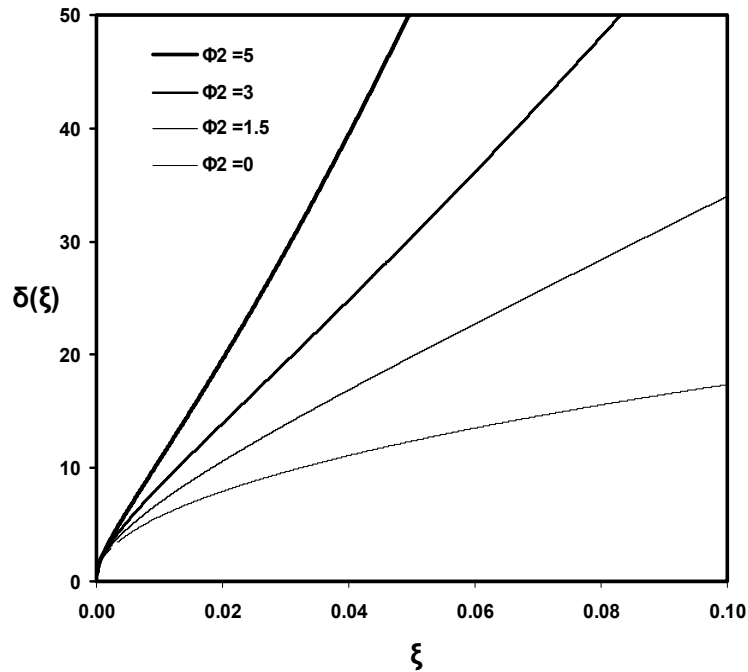


Figure 9.3 Dimensionless boundary layer thickness for different values of the heat generation source term

Figure 9.3 illustrates the effect of Joule heating on the dimensionless boundary layer thickness along the axial coordinate, ξ , for different values of the source generation term, ϕ^2 . In terms of the same ϕ^2 values, there are two trends observed: the first is described by $\phi^2 < 3$ values and the second by $\phi^2 \geq 3$ values. The first trend follows the qualitative behavior of the temperature variation described in figure 3, above. In other words, a single identifiable region that emulates an inverse exponential function is also observed in the variation of the dimensionless boundary layer thickness, δ^+ , for low ϕ^2 values. In addition, steady slope variations of δ^+ are observed for ξ values of approximately greater than 0.01 while a steeper variation of δ^+ develops near the electrode origin; this is for ξ values of smaller than 0.01. Finally for the second trend, high ϕ^2 values, the general variation in the boundary layer thickness, δ^+ , is a straight line where the exponential type of behavior is completely missing.

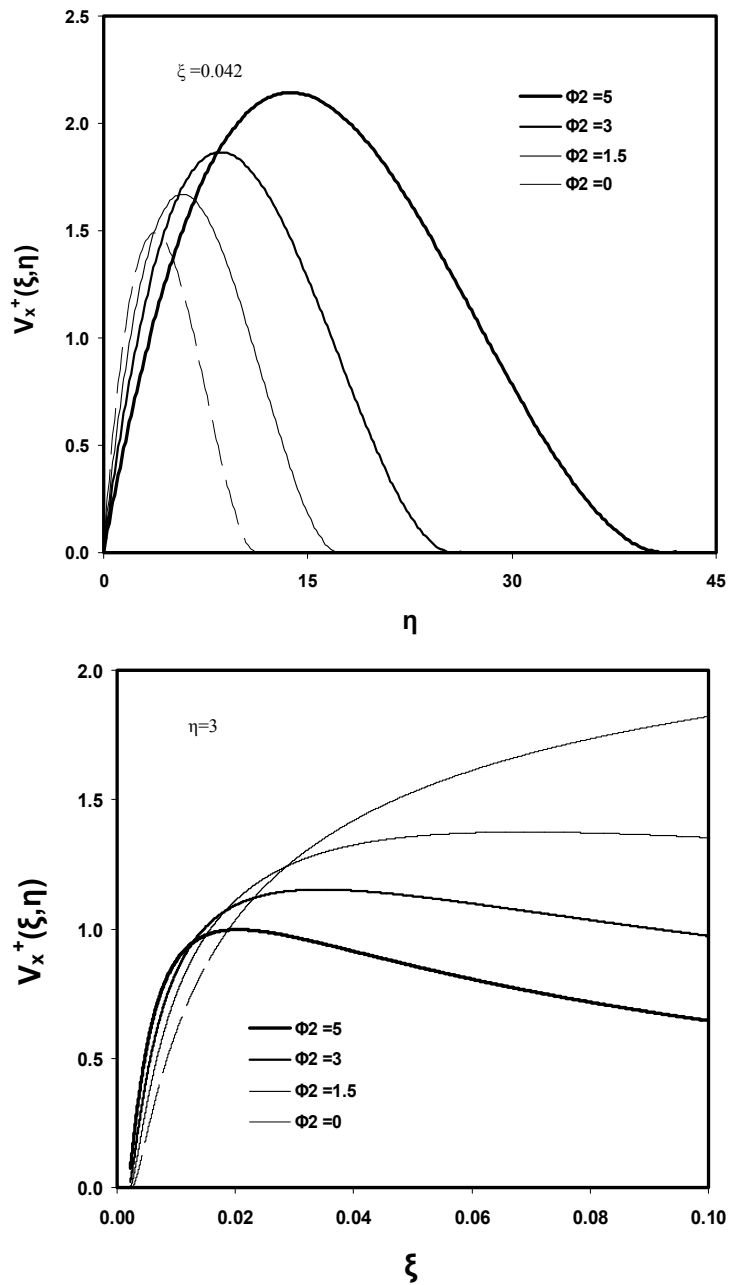


Figure 9.4 Dimensionless total velocity profiles showing the effect of the heat generation inside the boundary layer. Case of $\xi=0.042$ for the η -direction (a) and case of $\eta=3$ for the ξ -direction (b)

Figure 9.4 (a) shows the development of different dimensionless axial velocity profiles, induced by Joule heating generation, along the transversal axes, η , inside the boundary layer domain, for a given position in the axial direction, ($\xi=0.042$). Additionally, the figure exhibits for all the selected ϕ^2 values a family of curves that mimic a parabolic type shape (as proposed by the von Karman model) with a slowly decaying end at the region far away from the electrode. On the other hand, for all selected ϕ^2 values the dimensionless axial velocities at the surface of the electrode stay at the value of $V_x^+ = 0$. This is in agreement with the non-slip boundary condition of zero velocity at the electrode surface. Particularly, for a value of ϕ^2 equal to 5.0 the dimensionless axial velocity has a maximum of $V_x^+ = 2.14$ at approximately $\eta=14$. This is 1.4 times the value that corresponds to the η point for the no Joule heating effect ($\eta=4$) and it represents a 44% increase in velocity from the no heating effect case. The same analysis with ϕ^2 value of 3.0 generates a maximum velocity of $V_x^+ = 1.86$ at $\eta=9$, a 25% increase in the velocity from the maximum for the no Joule heating effect case. For the case of ϕ^2 equal to 1.5, the value of η at the maximum velocity is 50% more than the case of no Joule heating effect and the point represents an increase of 12% on the velocity magnitude. From this analysis, clearly the sensitivity of the system to the Joule heating effect is reasonably high and practical cases without accounting for Joule heating generation will occur in a significant error in velocity predictions.

Figure 9.4 (b) depicts dimensionless axial velocity profiles variation along the axial coordinate ξ for a given position of η ($\eta=3$). The general trend indicates that higher ϕ^2 values, first, proportionally increase velocity profiles toward individual maxima and, later, proportionally reduce the magnitude of velocity for any ξ value beyond these maxima. On the other hand, the $\phi^2 = 0$ value, no heat generation case, describes a semi-parabolic type curve reaching a maximum velocity without decay beyond this point. In particular, velocity profiles affected by heat generation are greater than expected without Joule heating effect along the axial coordinate ξ until they reach a point of equality. Beyond this point all the velocity profiles are smaller than those corresponding the without heating effect. A cross sectional analysis of the axial velocity on $\xi = 0.04$ for $\phi^2=1.5$, $\phi^2 = 3.0$, and $\phi^2 = 5.0$ values yields

velocity decay of 7%, 19%, and 36% respectively with respect to the value for the case of no Joule heating generation.

9.7 Summary of the Chapter

The main focus of this chapter is the analysis of the electrokinetic applications where Joule heating may be of importance. In particular, the region of interest for this study is the zone near vertical electrodes of rectangular geometrical aspect. The analysis is conducted for boundary layer flows caused by natural convection due to heat generation. The heat source in the electrokinetic cell is present because of a Joule heating effect due to an electrical field applied around the electrodes for cleaning purposes. The subject has been approached considering a number of steps as described below.

First, a modeling approach is used to emulate the boundary layer flow in the system. This mathematical description of the system under study is conceived by developing the heat transfer model, the continuity equation and the hydrodynamic model. The result of this approach is a set of two partial differential equations mutually coupled.

Second, the integral approximation developed by Von Karman is applied to the partial differential equations to make possible the solution of the system. After the integral boundary layer model has been derived, simplified expressions are obtained using profiles for velocity and temperature fields. A numerical solution of the differential model equations yields the temperature profile, the boundary layer thickness, and the component of the velocity field along the axial and transversal directions of the vertical electrode.

Finally, the effects of the heat generation on temperature and velocity profiles as well as on the boundary layer thickness are simulated, for different scenarios, and discussed. The implications of possible convective mixing effects near the electrode region are highlighted.